

CONCERT–Japan Research and Innovation Joint Call

Efficient Energy Storage and Distribution
Resilience against Disasters

RAPSODI Project

Risk Assessment and design of Prevention Structures
for enhanced tsunami Disaster resilience

Deliverable D5 – Computed
tsunami parameter values in
shallow waters and around
structures
2nd year of funding

20120768–05–R
30 June 2015
Revision: 0



This work was supported by funding received from the
CONCERT–Japan Joint Call on Efficient Energy Storage
and Distribution/Resilience against Disasters



Project information

Name of the project:	RAPSODI
Start of the project:	01 July 2013
Duration (no. of months):	24
End of the project	30 June 2015
Name and country/region of each partner	NGI, Norway; PARI, Japan; TU-BS, Germany; METU, Turkey
Overall budget	383 k€

Client

Client:	CONCERT-Japan Joint Call Secretariat
Client's contact persons:	CONCERT-Japan Coordinator The Scientific and Technological Research Council of Turkey (TUBITAK) Ms. Filiz Hayirli (filiz.hayirli@tubitak.gov.tr) concertjapan@tubitak.gov.tr Phone: + 90 312 468 5300 (ext.1910)
	CONCERT-Japan Joint Call Secretariat Centre national de la recherche scientifique (CNRS) Ms. Lucie Durocher (lucie.durocher@cns-dir.fr) Phone: + 33 (0)1 44 96 47 14 Fax: + 33 (0)1 44 96 48 56

Contract reference:	http://www.concertjapan.eu NGI 229578/H20; METU 113M556; TUBS 01DR13016;
Settlement numbers:	PARI 2013 H25国際第1-33号 2014 H26国際第1-17号

For NGI

Project manager:	Carl B. Harbitz
Prepared by:	Utku Kânoğlu and Naeimeh Sharghivand
Reviewed by:	Carl B. Harbitz

Publishable summary

After recognizing tsunamis as a significant hazard for coastal communities, inundation distance and, at most, flow depth were considered as significant products for tsunami hazard assessment. Hence, inundation maps were prepared showing only maximum inundation extent. Transoceanic tsunamis of early 21st century, such as 2004 Indian Ocean, 2010 Chile, and 2011 Japan tsunamis, have shown importance of tsunami currents, in particular at ports. Therefore, along with inundation depth, different metrics are in consideration to assess the tsunami hazard in coastal communities. Here, we provide a brief summary of exiting studies in the field. Recently, the American Society of Civil Engineers (ASCE) completed a chapter on "Tsunami Loads and Effects" for the updated ASCE 7-16 Standard, *Minimum Design Loads and Associated Requirements for Buildings and Other Structures*. This would help to design the structures as tsunami resistant and would help to create tsunami resilient communities.

NGI



Contents

1	Introduction	6
2	Recommended damage metrics	7
3	Tsunami impact forces	12
4	Numerical modeling of the tsunami currents	13
	4.1 Modeling with ComMIT	16
	4.2 NAMI DANCE modeling results	21
	4.3 FVCOM modeling results	27
	References	30

Review and reference page

NGI



1 Introduction

In order to identify zones potentially at high tsunami hazard it is important to determine metrics that characterize the tsunami impact. Tsunamis could penetrate to a great distance inland (inundation) and its time scale makes it a highly transient flow (Yeh et al., 2005). However, there is a limited guidance on tsunami impact other than runup, i.e. inundation. Especially, it is essential to understand tsunami behavior in the inundation zone for design codes.

There are several examples of tsunami behavior in the inundation zone. As given in Yeh et al. (2005), affect of the 1960 Chilean tsunami at several Japanese coastal towns and the 1964 Alaska tsunami in Port Alberti, Canada, show a gradual rise and fall of water with no wave breaking as a result of very long incoming waves. However, again following Yeh et al. (2005), often tsunamis break offshore creating surging. Tsunami might break directly onto structure, which could be considered similar to a collapsing breaker. One example of this is destruction of Scotch Cap Lighthouse during the 1946 Aleutian tsunami (Okal and Hebert, 2007; Fryer et al., 2004).

Yeh et al. (2005) outline forces on structures for the development of design guidelines for tsunami vertical evacuation structures. Considering Yeh et al. (2005), and a limited number of other studies and publications on the subject, the useful parameters that are of interest in assessing tsunami impact are maximum wave elevation, minimum wave elevation, maximum flow depth, flow velocity, front velocity, maximum current speed, maximum momentum flux, Froude number, hydrostatic force, buoyant force, hydrodynamic force, surge force, impact force, and breaking wave force (see also RAPSODI Deliverable 1 “Existing tools, data, and literature on tsunami impact, loads on structures, failure modes and vulnerability assessment”, METU 2015).

Figure 1 shows the basic parameters used to calculate the damage metrics; $d(x,y)$ denotes bathymetric or topographic height with respect to an undisturbed mean sea level, here, following the sign convention, $d(x,y) > 0$ in the sea (bathymetry) while $d(x,y) < 0$ in the land (topography).

The elevation of the water level above the undisturbed mean sea level at spatially (x,y) and temporarily at t is denoted by $\eta(x,y,t)$, and the time dependent inundation depth (flow depth) is defined as

$$h(x,y,t) := \eta(x,y,t) + d(x,y). \quad (1)$$



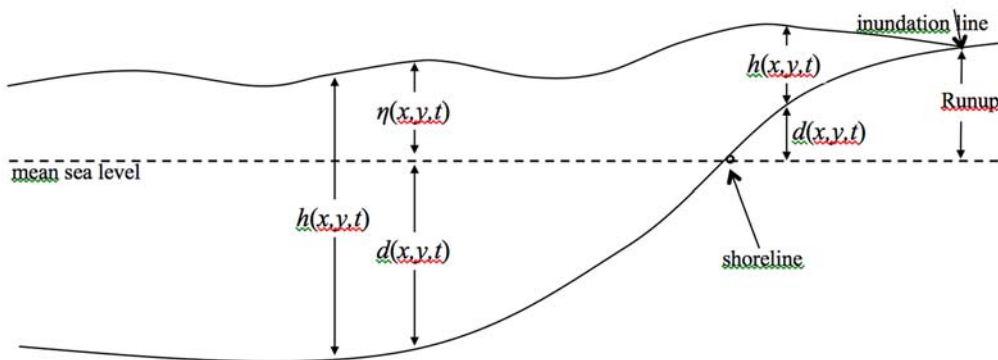


Figure 1: Schematic representation and basic definitions.

2 Recommended damage metrics

The following damage metrics can be computed once water elevation $\eta(x, y, t)$, flow depth $h(x, y, t) := \eta(x, y, t) + d(x, y)$, and velocity components $v(x, y, t)$ and $u(x, y, t)$ are calculated through a numerical model.

- **Maximum wave elevation**, i.e.,

$$\eta_{\max}(x, y) := \max_t \eta(x, y, t). \quad (2)$$

In particular, the elevation of maximum penetration (inundation line), which is referred as runup, is important in hazard planning.

- **Minimum wave elevation**, i.e.,

$$\eta_{\min}(x, y) := \min_t \eta(x, y, t). \quad (3)$$

- **Maximum flow depth**, i.e.,

$$h_{\max}(x, y) := \max_t h(x, y, t), \quad (4)$$

which is calculated only at inland, i.e., for $d(x, y) < 0$.

- **Maximum current speed**

Let $\vec{V}(x, y, t)$ denote the velocity vector, and $u(x, y, t)$ and $v(x, y, t)$ denoting its x and y components, respectively. Then, current speed $V(x, y, t)$ is

$$V(x, y, t) := \sqrt{u^2(x, y, t) + v^2(x, y, t)}. \quad (5)$$

Then maximum current speed is calculated at each grid point for entire duration of an event:

$$V_{\max}(x, y) := \max_t V(x, y, t) = \max_t \left\{ \sqrt{u^2(x, y, t) + v^2(x, y, t)} \right\}, \quad (6)$$

The maximum current speed is calculated in the unit of m/s.

Evolution of two different waveforms over a simple geometry of sloping beach as described by Kânoğlu (2004) or Kânoğlu and Synolakis (2006) is shown in Figure 2. As shown in Figure 2, the highest velocity does not occur close to the location of the highest flow depth location, even for propagation over a simple geometry of a sloping beach. Also, the highest velocity, hence highest momentum flux, can occur during tsunami withdrawal. Furthermore, the region of highest velocity depends on the incoming waveform, i.e., the particular scenario under study. Therefore, currents cannot be neglected in tsunami hazard assessments. Also, the associated kinetic energy can be the most destructive aspect of a tsunami. This is important since very high currents can be associated with relatively modest flow depth. In particular, for certain locations, regions of high currents might not correspond to regions of high flow depths. This frequently occurs in river entrances and adjacent bay areas. Therefore, the lack of correspondence between maximum flow depth and currents means that inundation maps with maximum flow depth could be dangerously misleading. If only high flow depths are taken into account and destructively high currents are not, the overall tsunami hazard and destructive potential could be seriously underestimated in areas of modest wave height. Hence, a more complete hazard assessment must employ *impact indices* or *impact metrics* that consider both potential (wave height) and kinetic energy (current).

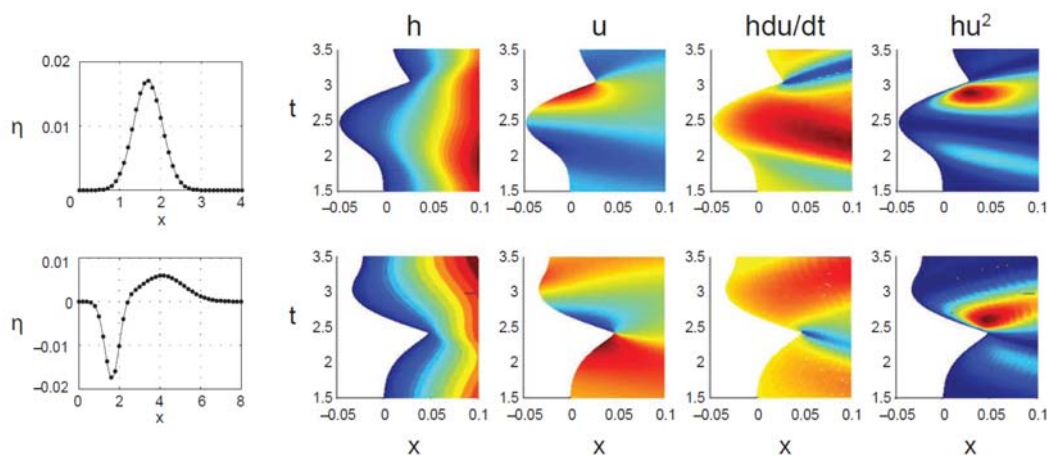


Figure 2: Evolution over time, t , of the total water height (h), velocity (u), hdu/dt , and hu^2 as a function of the onshore variable x of a simple sloping beach, as evaluated by Kânoğlu and Synolakis (2006) for two different initial waveforms, i.e., Gaussian and leading-depression Gaussian. The color scale is relative, with blue representing relatively small values and red representing relatively large values.

- **Specific maximum momentum flux per unit width**

$$M_{\max}(x, y) := \max_t \{h(x, y, t) \cdot V^2(x, y, t)\}, \quad (7)$$

The specific maximum momentum flux per unit width is calculated in the unit of m^3/s^2 .

- **Froude number**

Hydrodynamic demand (HD) is a dimensionless parameter represented as the ratio of hydrodynamic force –drag force– (exerted by the flow) to hydrostatic force onto the structure. Hydrostatic force can be taken as a reference force in order to obtain comparative dimensionless value for hydrodynamic force. The normalization of hydrodynamic force by hydrostatic force gives

$$\begin{aligned} HD &= \frac{F_D}{F_h} = \frac{\frac{1}{2} C_D \rho_w A V^2}{\frac{1}{2} \rho_w g h A} \\ &= C_D \frac{V^2}{g h}. \end{aligned} \quad (8)$$

Here C_D is the drag coefficient and A is the projected area of the body on the normal plane to the flow direction. Since, the Froude Number F_R is defined as V/\sqrt{gh} , damage metrics can be represented as

$$HD = C_D * F_R^2. \quad (9)$$

It is recommended to calculate F_R for the values of $h \geq 0.01$ m to avoid the singularities. The drag coefficient C_D depends mainly on structure shape and secondarily the flow conditions. It describes characteristic amount of hydrodynamic drag caused by water flow. Two objects having the same frontal area and exposed to same flow velocity will experience a drag force proportional to their C_D values. Drag coefficient for same shaped structures can change with the Reynolds number (a dimensionless number that is the ratio of the inertial force of the medium over its viscous force) and also with the roughness of the surfaces. Table 1 summarizes suggestions for the value of drag coefficient C_D given in Federal Emergency Agency (FEMA) Coastal Construction Manual (CCM, 2000) and Synolakis (2003).



Table 1: FEMA CCM suggestions for the value of drag coefficient C_D .

Structure Type	C_D value
Square or rectangular piles	2.0
Round piles	1.2
Large obstructions based on width (w) to flow depth (h) ratio	1.25 for $w/h < 12$ $1.3 < C_D < 1.8$ for $12 < w/h < 120$ 2.0 for $w/h > 120$

- **Front velocity**

The front velocity is the speed of the tip of the tsunami wave. This could be evaluated as speed of fluid particle of last wet point at numerical calculation. This is important since field observations demonstrated that the wave-front appears to slow down as it approaches the shoreline. This leads to a sense of false security. One can easily imagine that it could be outrun, but short time later (depending on location), the wave-front accelerates rapidly as the main disturbance arrives.

Fritz *et al.* (2006), investigating a video taken near the Grand Mosque in Aceh during the 2004 Indian Ocean tsunami, infer that the wave front first moved at speeds less than 8km/h, then accelerated to 35km/h. The same phenomenon is probably responsible for the memorization of victims during tsunami attacks. The 2004 Boxing Day tsunami prompted hundreds of photos, some found in cameras that were washed by the tsunami. At the time of the picture-taking, tsunami was just offshore, people appear to pose in front of the advancing wave-front in many of these photos. Why didn't these people run away as they saw the tsunami advancing, instead thought they had the time to take pictures? This might be first noted in series of photographs of the 1946 Aleutian tsunami approaching Hilo, Hawaii. A series of two photographs (Figure 3) from the 1995 Manzanillo, Mexico, tsunami taken by survivor which show three men being unable to outrun a very thin wave-front underscores this point (Borero *et al.*, 1997).

This effect of wave-front acceleration was first shown by Synolakis (1986) analytically, and later it is implicit in the work of Carrier *et al.* (2003) and Kánoğlu (2004). However, acceleration of the wave front passing the initial shoreline was not entirely recognized until pictures from events were examined. Synolakis (1987) showed that, first, the front of the solitary wave slows down as it climbs up the sloping beach, due to the reduction in depth (Figure 4). Once the wave hits the initial shoreline, it slows down, but accelerates again, before decelerating to its ultimate on land penetration point (inundation line), the maximum wave runup. Zelt and Raichlen (1991) also studied front velocities experimentally and numerically over an impermeable bed by incident solitary waves.





Figure 3: Advancing of wave-front on La Manzanilla in the southern end of Tenacatita Bay after the 1995 Manzanillo, Mexico, tsunami. The water had advanced more than 100 m when the lower photo was taken. Eyewitnesses reported that the wave traveled about as fast as a person could run. After Borerro et al. (1997).

NGI



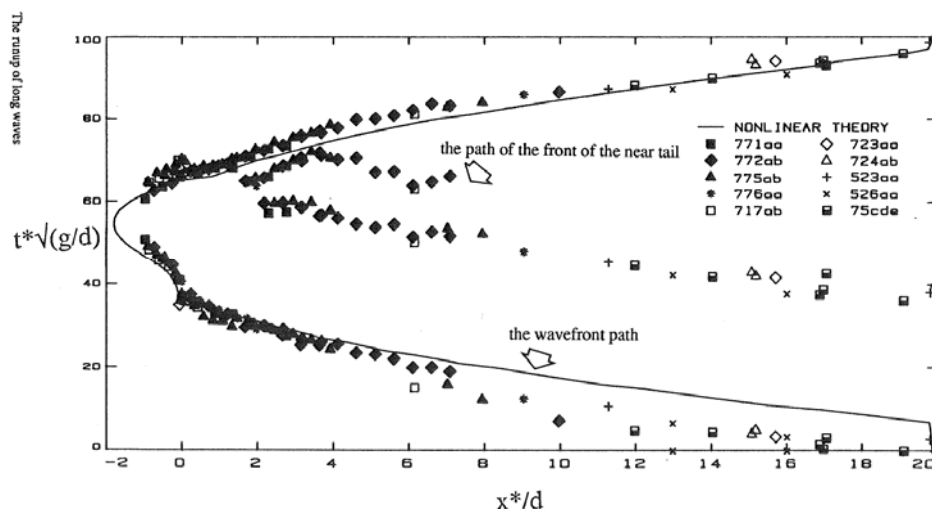


Figure 4: The path of the wave-front and of the tail of a 0.0185 solitary wave up a 1:19.85 beach. Comparison between the nonlinear analytical model and experiments. Different symbols indicate different realizations of the same experiment. After Synolakis (1987).

3 Tsunami impact forces

Tsunamis can generate large onshore currents that can cause dramatic damage to structures and even move large objects far inland. The 26 December 2004 Indian Ocean and 11 March 2011 Japan mega-tsunamis demonstrated tsunami impact on structures in a rather dramatic fashion. As mentioned above, high currents can be associated with relatively modest flow depth, e.g. in river entrances. During the 1994 Mindoro Philippines tsunami, in an area where the vertical inundation heights did not exceed 3 m (10 ft), the tsunami floated a 6000 ton generating barge, broke its mooring lines and carried it as much as 1 mile upstream the Baryan River.

All structures in coastal high hazard zones should be designed and constructed to resist flotation from tsunamis. The forces and effects of floodwaters on the structures should be considered and evaluated whenever designing the buildings and structures in potential flood zones. According to the Yeh *et al.* (2005) the following forces must be examined and considered in the construction of buildings and structures at high-risk coastal areas (refer to Yeh *et al.* (2005) for more detailed descriptions):

- **Hydrostatic Forces:** This is due to an imbalance of pressure from difference on water depth on opposite sides of a structure. Hydrostatic force can act laterally on an object.
- **Buoyant forces:** This force acts to partially or totally submerged objects and will act vertically through the center of mass of the displaced volume.
- **Hydrodynamic forces:** Hydrodynamic force will act to the structure due to water flow around a structure.



- **Surge forces:** When the leading edge of a surge of water impinging on a structure it causes surge force.
- **Impact forces:** When tsunami inundates, e.g. shore boats, pieces from houses, cars, other debris, etc., are transported and strike other structures and this will cause impact forces.
- **Breaking wave forces:** Here two breaking wave load conditions are of interest; wave breaking on small-diameter vertical elements and wave breaking against walls.

One recent example is presented in O'Brien *et al.* (2015) considering effect of forces caused by tsunamis on oscillating wave surge converters. Recently, the American Society of Civil Engineers (ASCE) 7 Tsunami Loads and Effects Subcommittee is presently completing a comprehensive chapter with the ASCE/SEI 7 Standard, Minimum Design Loads for Buildings and Other Structures (ASCE, 2016). This would become the first US tsunami design provisions established.

4 Numerical modeling of the tsunami currents

Recently, the United States National Tsunami Hazard Mitigation Program (NTHMP) organized Mapping & Modeling Benchmarking Workshop: Tsunami Currents (February 9-10, 2015 at Portland, Oregon), for validation and verification of tsunami numerical models for tsunami currents (http://coastal.usc.edu/currents_workshop/index.html). Five benchmark problems were presented. Fourth benchmark problem was on experiment of a single long-period wave (similar to solitary wave, but not a solitary wave) propagating over piecewise linear slopes and then onto a 1:50 scale model of the town of Seaside, Oregon (Figure 5-6). The generated wave is a custom wave meant to maximize the stroke of the wave-maker, while generating a long period wave. Due to this generation approach, generated wave is a solitary like wave. The location of wave-maker is shown in Figure 5. Initial wave could be imposed either as a wave maker motion or as an initial wave profile at wave gauge locations WG1 and WG2, as presented in Figure 7 (Table 1). Initial waveform, which is used in numerical model, could be compared with measurements at WG3 and WG4 to make sure model mimics experimental setup. Free surface elevation and velocity measurements were recorded at several locations (Table 2). Purpose of this benchmark problem was to compare free surface height, velocity, and momentum flux at several locations (Figure 8, Table 2). Refer to Park *et al.* (2013) and workshop webpage for detail description of the experimental setup.



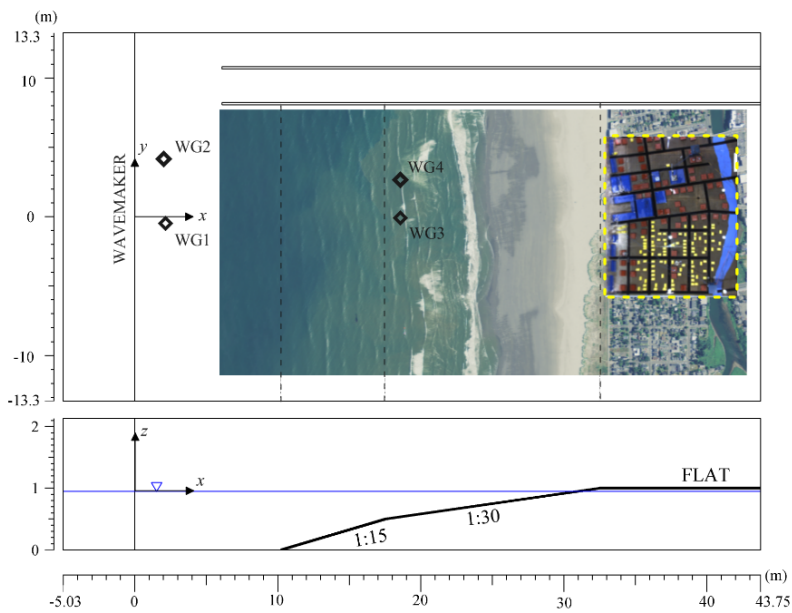


Figure 5: Experimental model setup.

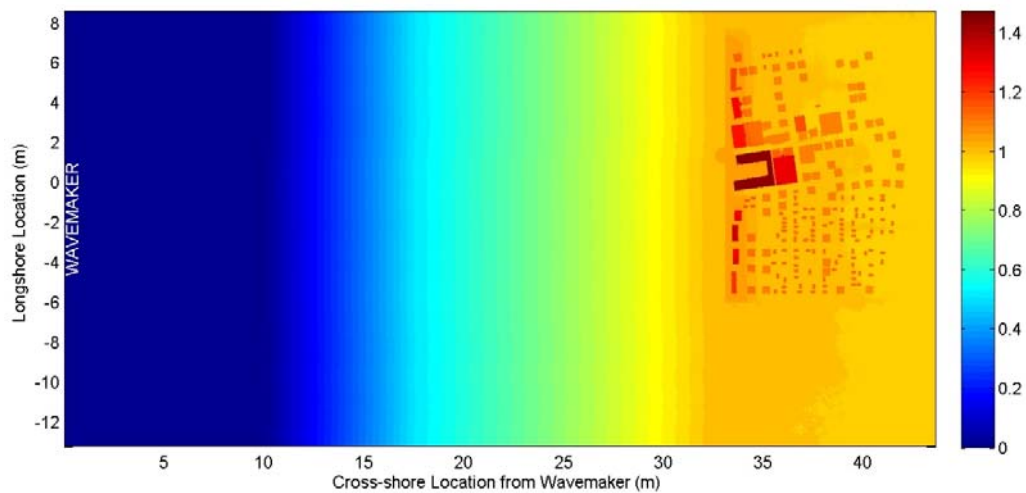


Figure 6: Representation of bathymetry in the laboratory scale.

Table 1: Wave gauge locations.

	X(m), Y(m)
Wave maker	0, 0
Wg1	2.068, -0.515
Wg2	2.068, 4.065
Wg3	18.618, 0
Wg4	18.618, 2.86



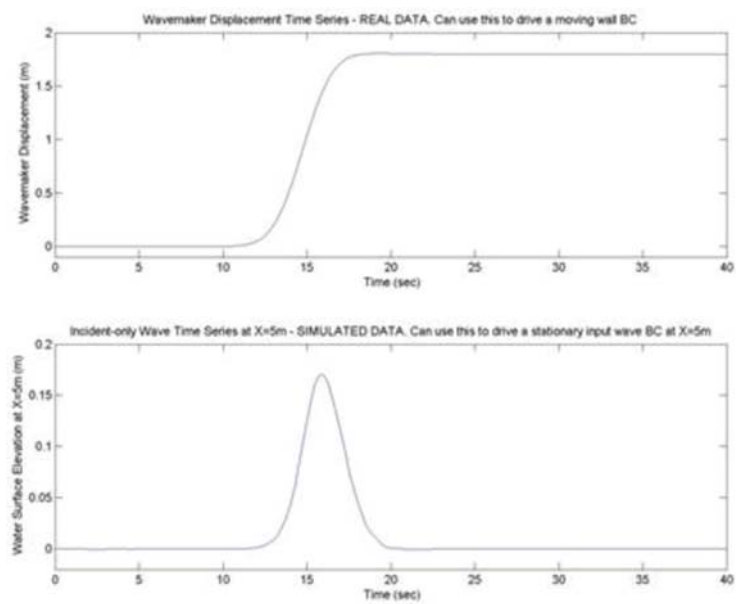


Figure 7: (Top) Wave maker displacement and (bottom) wave profile at WG1 and WG2.

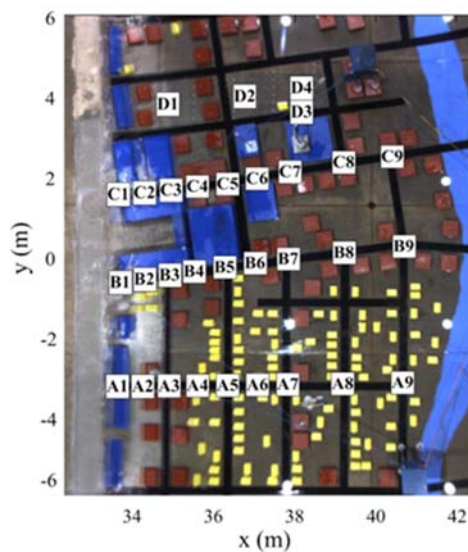


Figure 8: Locations of free surface and velocity measurements.



Table 2: List of free surface and velocity measurement locations.

The location of USWG and ADV on the flat section								
Position	USWG1/ADV1(A)		USWG2/ADV2(B)		USWG3/ADV3(C)		USWG4/ADV4(D)	
	X (m)	Y (m)	X (m)	Y (m)	X (m)	Y (m)	X (m)	Y (m)
1	33.611	-3.193	33.721	-0.588	33.809	1.505	35.124	3.712
2	34.103	-3.194	34.218	-0.533	34.553	1.604	36.684	3.888
3	34.534	-3.184	34.679	-0.467	35.051	1.686	38.086	4.070
4	35.040	-3.181	35.176	-0.406	35.556	1.769	38.141	3.585
5	35.544	-3.194	35.747	-0.317	36.050	1.845	N/A	N/A
6	36.355	-3.199	36.635	-0.229	37.047	1.988	N/A	N/A
7	37.767	-3.201	37.773	-0.068	38.243	2.193	N/A	N/A
8	39.223	-3.204	39.218	0.135	39.208	2.338	N/A	N/A
9	40.676	-3.228	40.668	0.269	40.400	2.582	N/A	N/A

This benchmark problem is modeled by Kânoğlu *et al.* (2015) using the Community Modeling Interface for Tsunamis (ComMIT), which is an interface to the validated and verified (Synolakis *et al.*, 2008, 2007) tsunami numerical model of the Method of Splitting Tsunami (MOST) (Titov and Synolakis, 1998, 1997, 1995). The problem is also modeled using NAMI DANCE, finite difference solution of the nonlinear shallow water equations, (NAMI DANCE, 2010) which is developed in collaboration with METU, Turkey and Special Bureau of Automation of Research Russian Academy of Sciences, Russia. Moreover, Wiyono (2015) has modeled the problem using Finite-Volume Community Ocean Model (FVCOM) (Chen *et al.*, 2006). Summary of results of the modeling efforts with the above models are presented here.

4.1 Modeling with ComMIT

Here, experimental set-up was up-scaled using the scaling ratio 1/50. Then, 3 m grid resolution has been used in the numerical modeling. Note that three nested grids at same resolution and extent have been used since ComMIT requires three nested grid structure. Figure 9 shows bathymetry used in modeling. Here, incident wave at WG1 and WG3 (Figure 10) are compared with experimental results to make sure model set-up is correct. Moreover, flow depth (h), velocity (V), and specific momentum flux per unit width (hV^2) at four wave gauge locations: WGB1, WGB4, WGB6, WGB9 (see Figure 8 for the wave gauge locations) are compared and shown in the Figures 11-14.



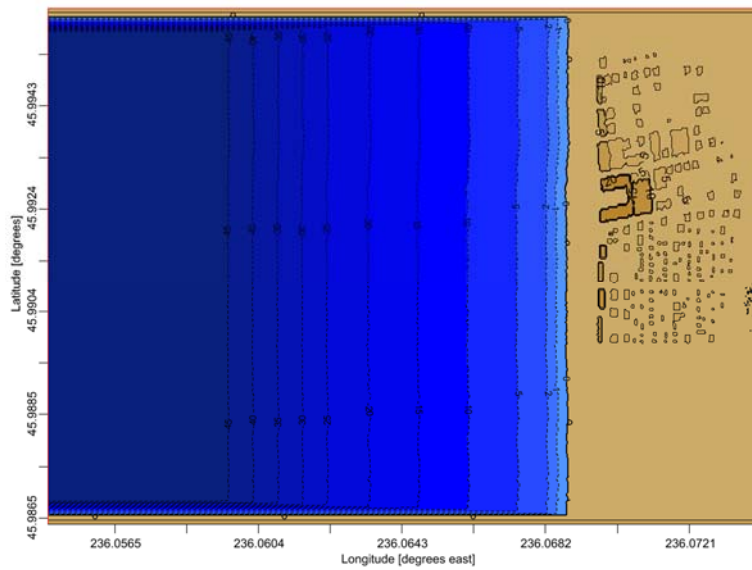


Figure 9: Representation of grid extent in ComMIT, i.e., A-, B-, and C-grids have the same extent.

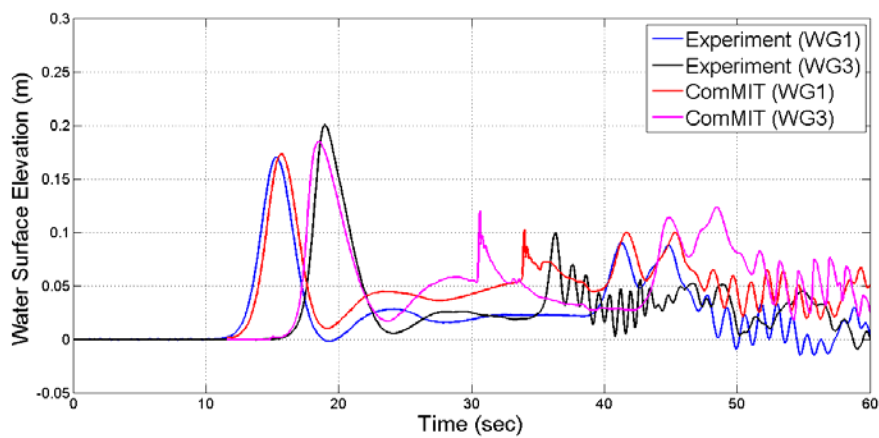


Figure 10: Incident wave comparisons at WG1 and WG3. For the location of wave gauges see Figure 5.



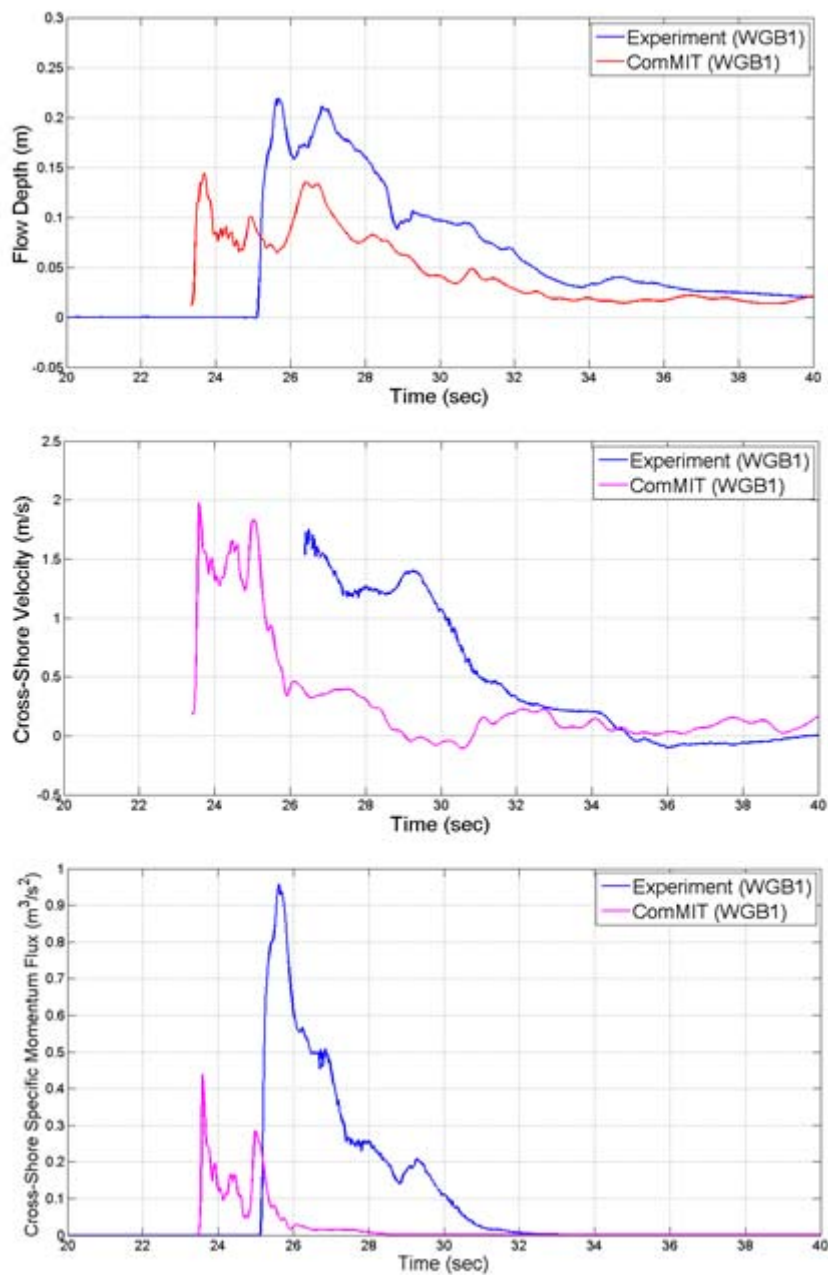


Figure 11: (Top to bottom) Flow depth, cross-shore velocity, and cross-shore specific momentum flux per unit width comparisons at WGB1 using ComMIT. See Table 2 and Figure 8 for the location of wave gauge.



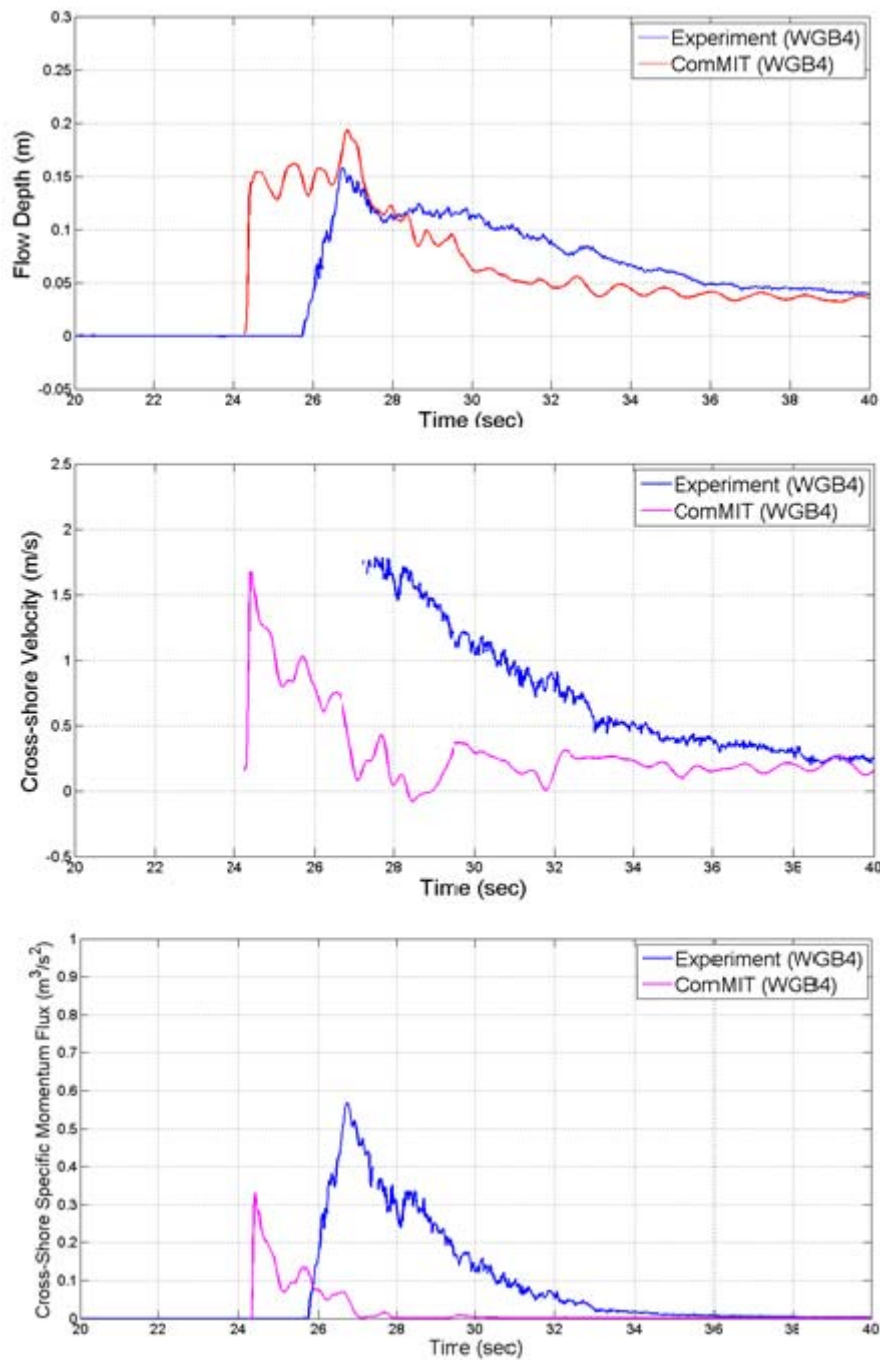


Figure 12: (Top to bottom) Flow depth, cross-shore velocity, and cross-shore specific momentum flux per unit width comparisons at WGB4 using ComMIT. See Table 2 and Figure 8 for the location of wave gauge.



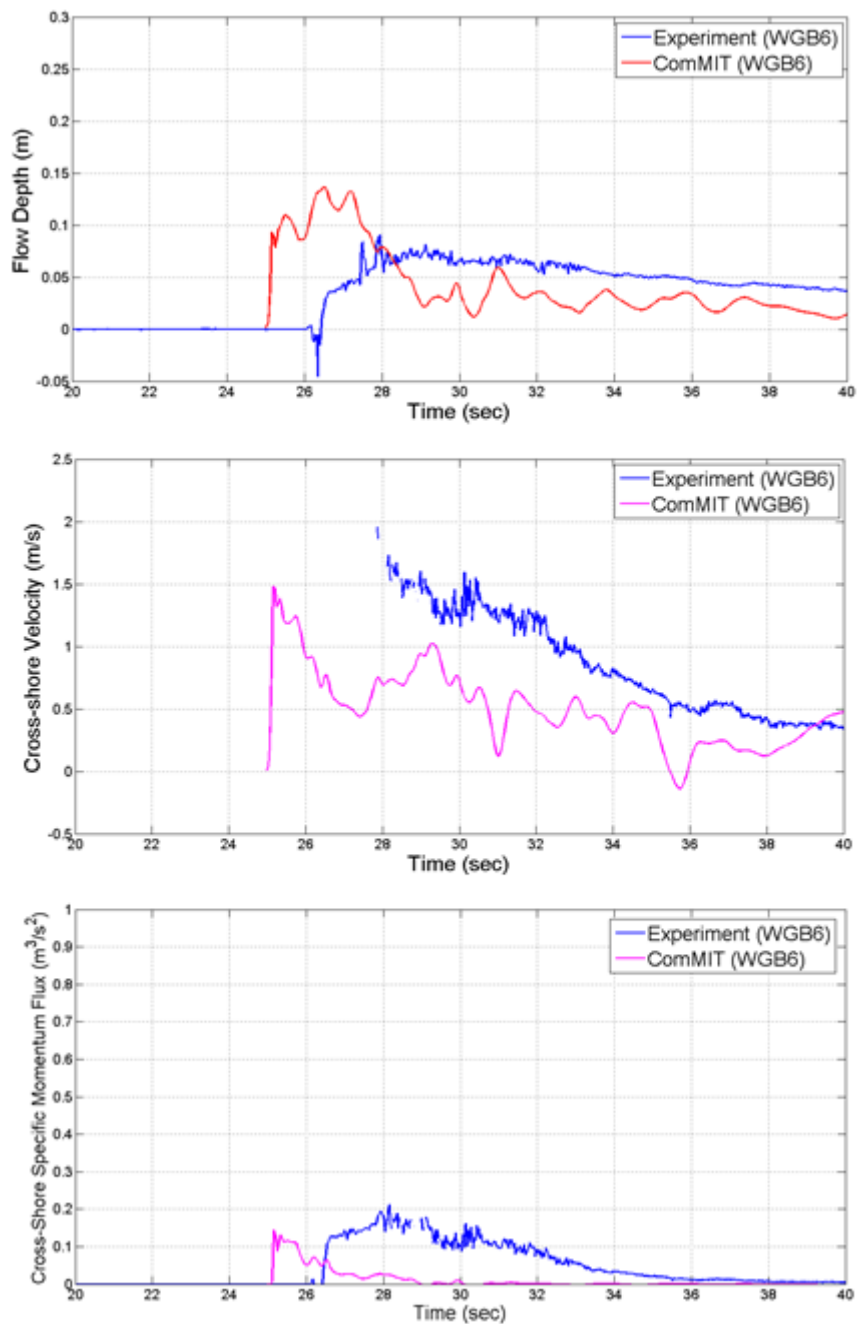


Figure 13: (Top to bottom) Flow depth, cross-shore velocity, and cross-shore specific momentum flux per unit width comparisons at WGB6 using ComMIT. See Table 2 and Figure 8 for the location of wave gauge.



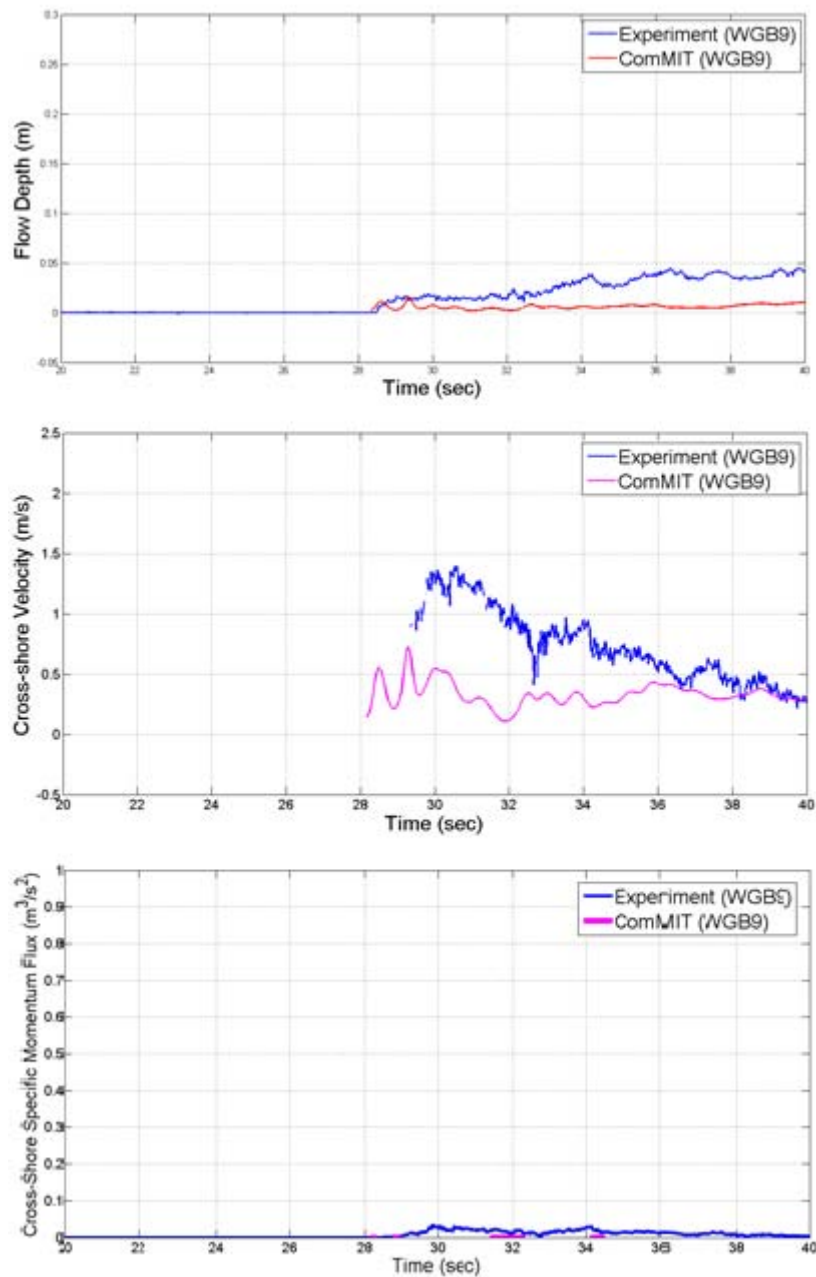


Figure 14: (Top to bottom) Flow depth, cross-shore velocity, and cross-shore specific momentum flux per unit width comparisons at WGB9 using ComMIT. See Table 2 and Figure 8 for the location of wave gauge.

4.2 NAMI DANCE modeling results

Tsunami numerical model NAMI DANCE is also applied for this benchmark problem (Yalciner, et al., 2015). 0.1m resolution has been used in NAMI DANCE modeling with the friction coefficient equal to zero. Here, initial condition is applied



at WG3 and comparison with experimental data has been shown in Figure 15. Moreover, the results for flow depth (h), velocity (V), and specific momentum flux per unit width (hV^2) at the four wave gauge locations: WGB1, WGB4, WGB6, and WGB9 are presented in Figures 16-19.

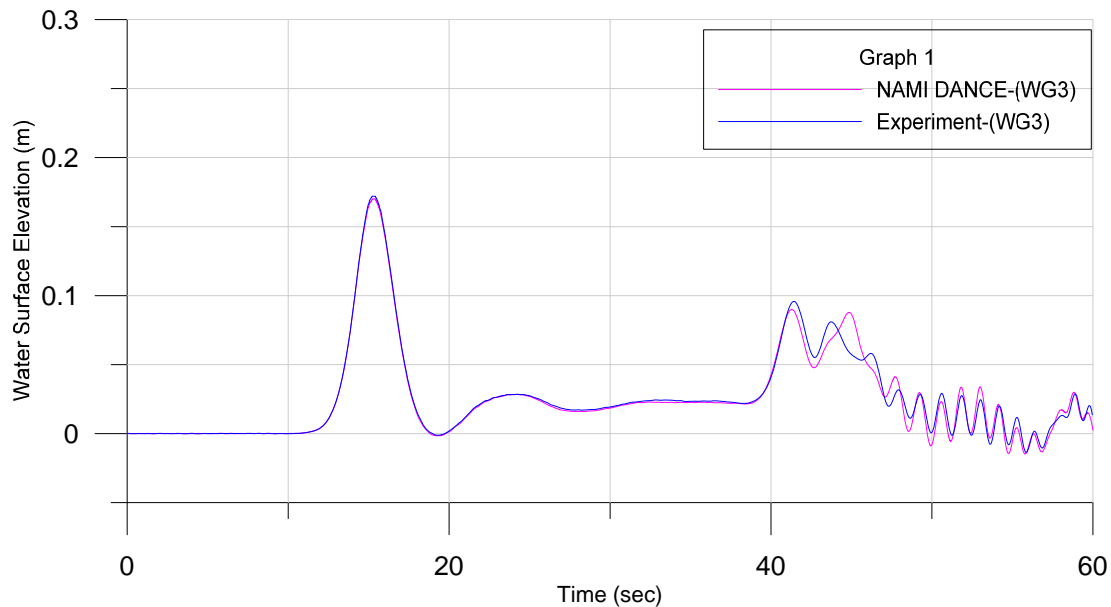


Figure 15: Incident wave comparisons at WG3.



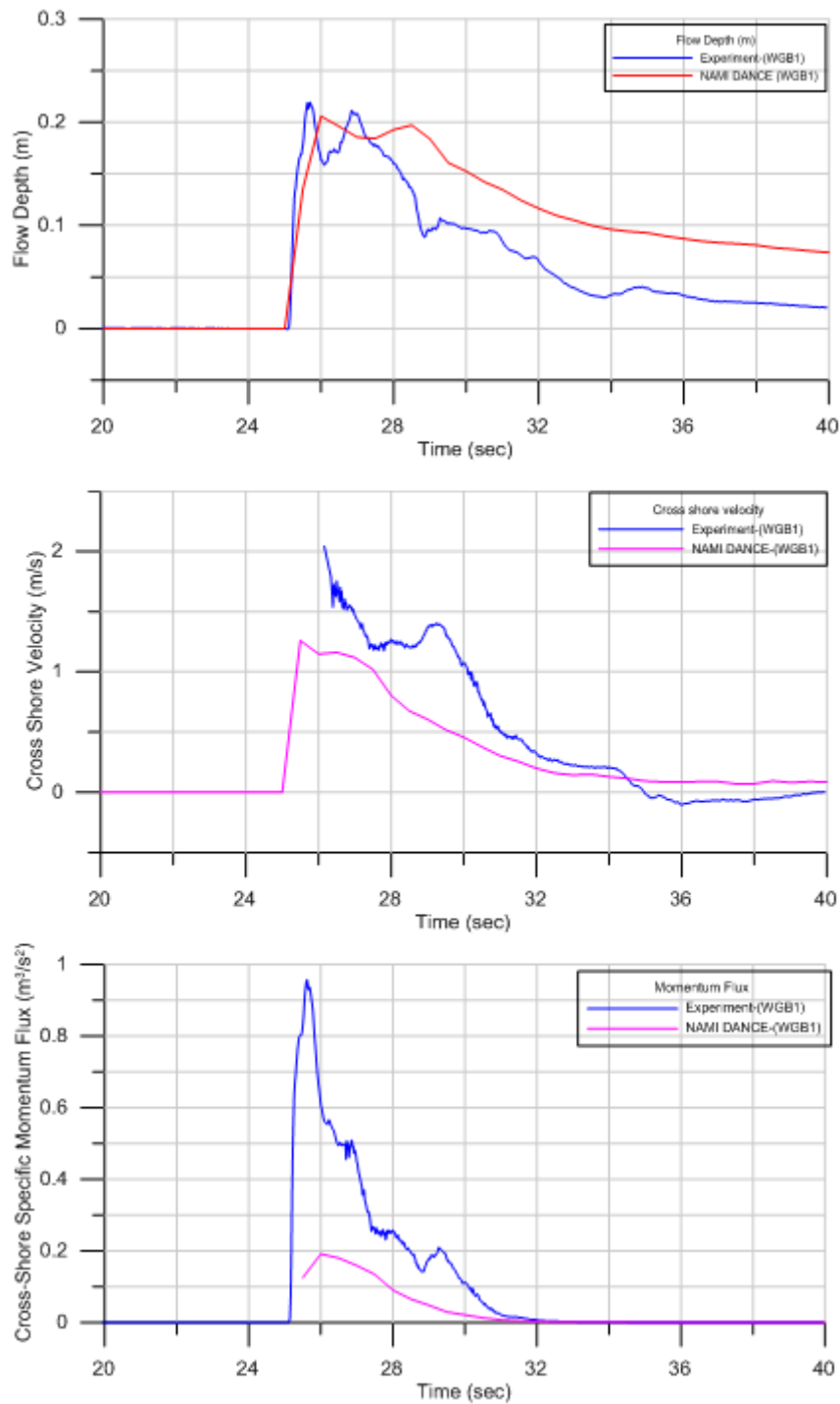


Figure 16: (Top to bottom) Flow depth, cross-shore velocity, and cross-shore specific momentum flux per unit width comparisons at WGB1 using NAMI DANCE. See Table 2 and Figure 8 for the location of wave gauge.



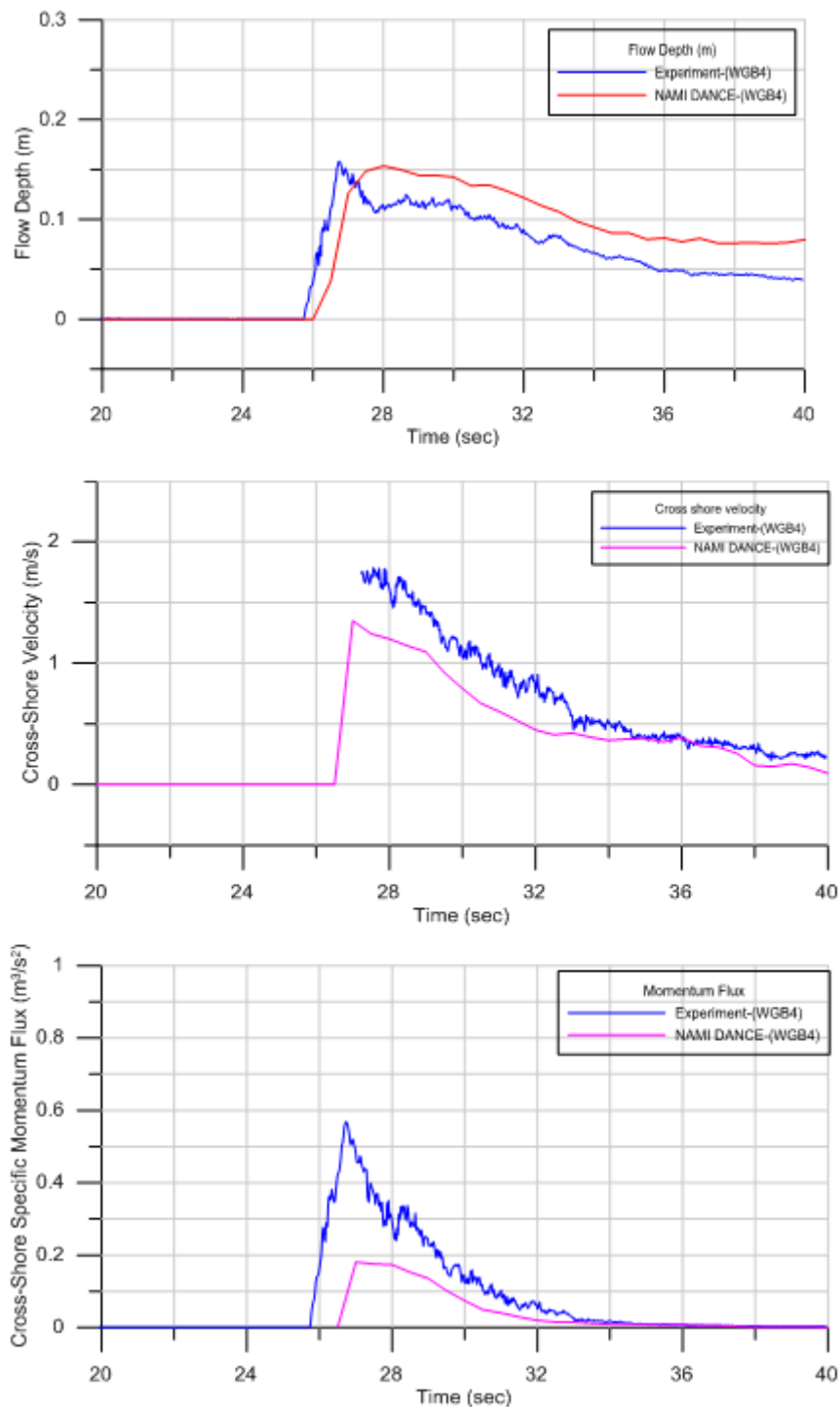


Figure 17: (Top to bottom) Flow depth, cross-shore velocity, and cross-shore specific momentum flux per unit width comparisons at WGB4 using NAMI DANCE. See Table 2 and Figure 8 for the location of wave gauge.



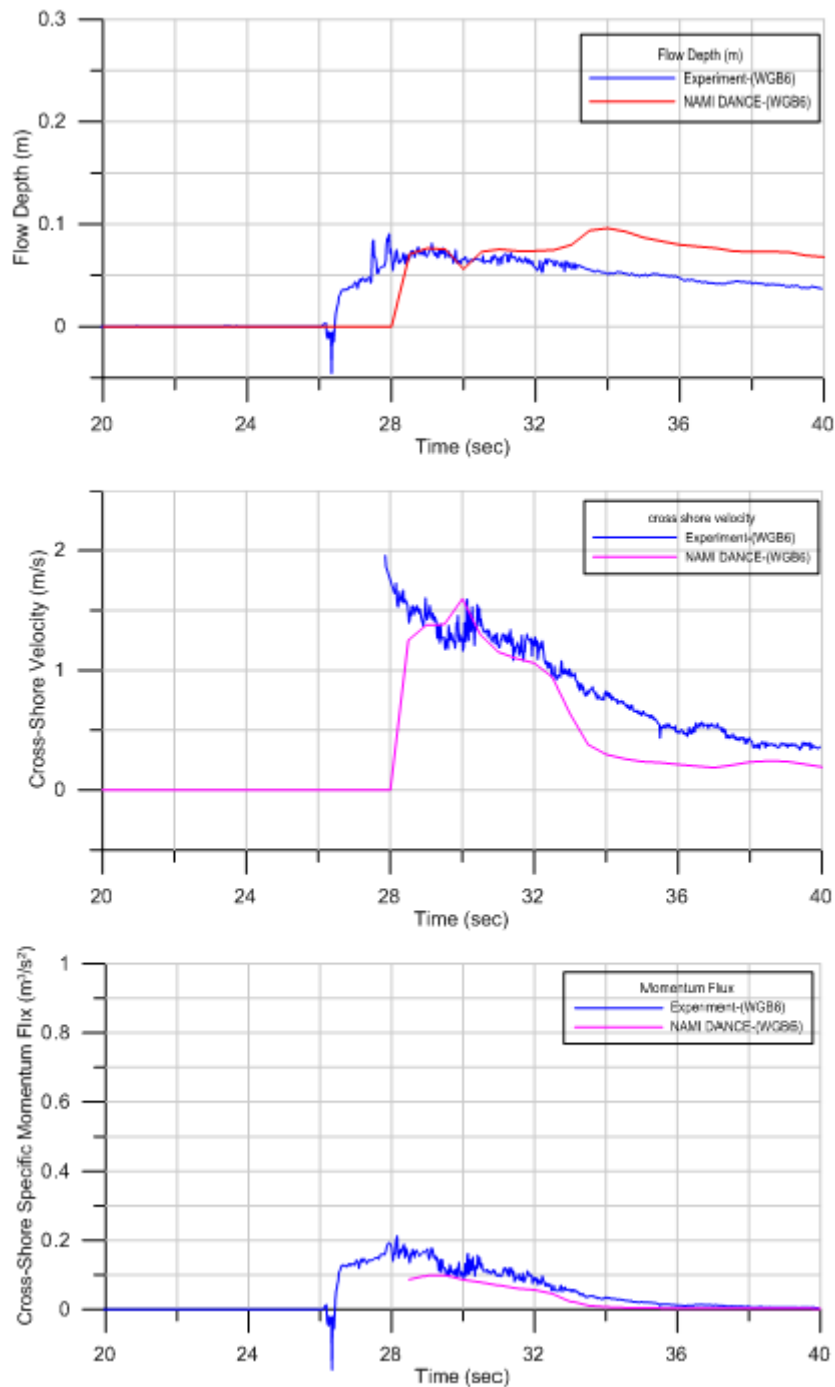


Figure 18: (Top to bottom) Flow depth, cross-shore velocity, and cross-shore specific momentum flux per unit width comparisons at WGB6 using NAMI DANCE. See Table 2 and Figure 8 for the location of wave gauge.



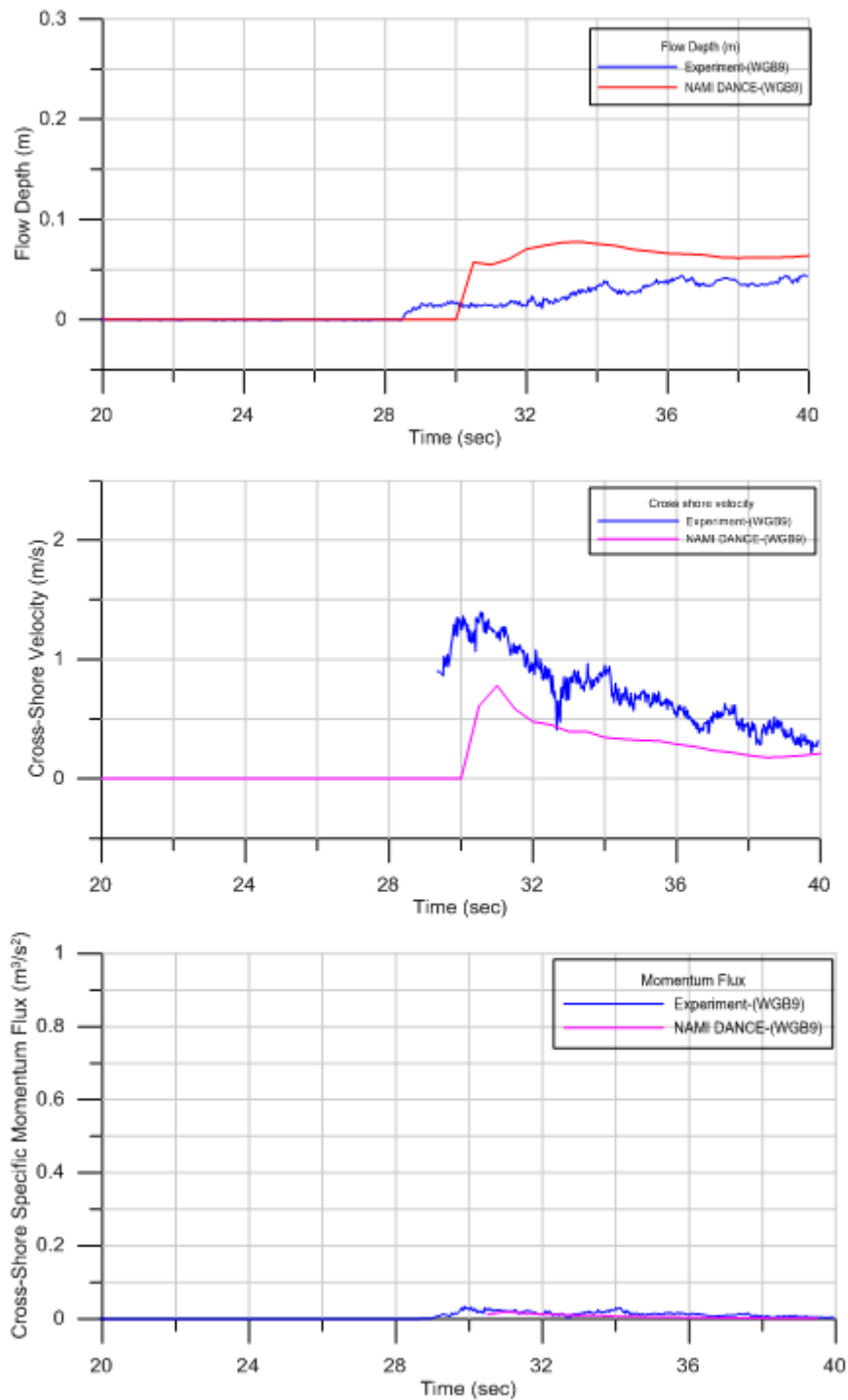


Figure 19: (Top to bottom) Flow depth, cross-shore velocity, and cross-shore specific momentum flux per unit width comparisons at WGB9 using NAMI DANCE. See Table 2 and Figure 8 for the location of wave gauge.



4.3 FVCOM modeling results

FVCOM (Chen *et al.*, 2006) is developed by the University of Massachusetts Dartmouth, Woods Hole Oceanographic Institution-WHOI joint efforts. Finite volume model FVCOM employs an unstructured grid using 3-D primitive equation coastal ocean circulation model. Wiyono (2015) performed tsunami numerical modeling for the benchmark problem 4 using FVCOM and some results will be presented here. Wiyono (2015) has used several unstructured grid mesh systems (with the grid size of 0.15 m) to perform sensitivity analysis for different cases, i.e., resolved mesh system, concrete-resolved mesh system, and unresolved mesh system.

Resolved mesh system is developed to construct an idealized case of the physical experiment. In this case all structures including concrete and wooden buildings are resolved. In the concrete-resolved mesh system only concrete buildings, i.e., large buildings are resolved, for the other structures, i.e., wooden buildings roughness coefficient parameters are included to show effects of buildings in the numerical modeling. In the third case, unresolved mesh system, no buildings are resolved, but roughness coefficient parameters are included for all buildings.

Comparisons between the experiment and numerical model incident waves are presented at WG1 and WG3 in Figures 20-21. In addition, flow depth and cross-shore velocity component comparisons are presented in Figures 22-24. Moreover, numerical model estimates and experimental measurements for inundation depth and velocity are compared at three wave gauge locations, WGB1, WGB4 and WGB6, and shown in Figures 22-24.

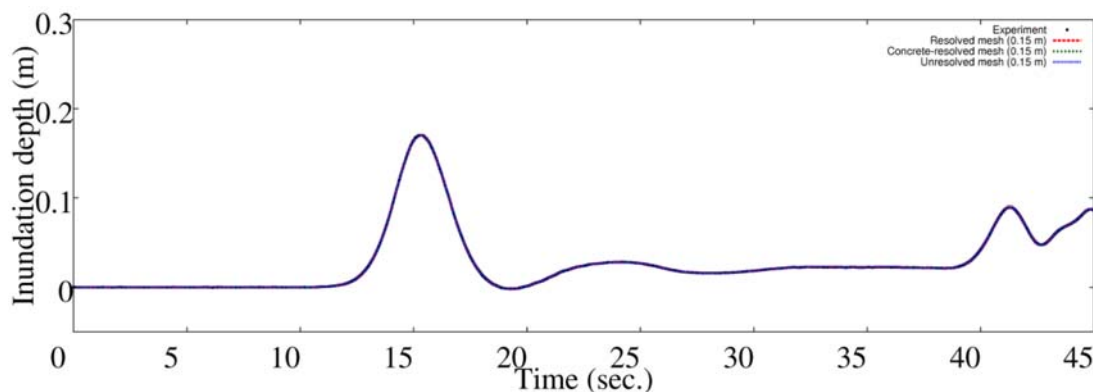


Figure 20: Incident wave comparisons at WG1. After Wiyono (2015). For the location of wave gauges see Figure 5.



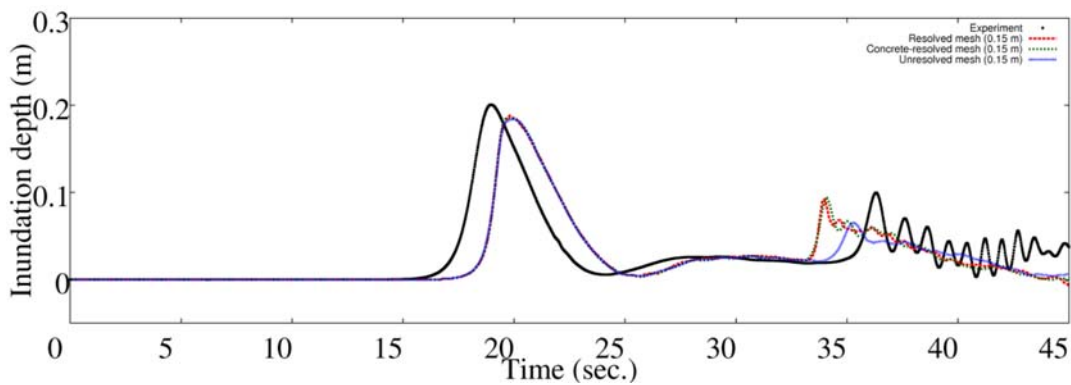


Figure 21: Incident wave comparisons at WG3, (black) experiment, (red, green, blue) numerical modeling in different resolutions. After Wiyono (2015). For the location of wave gauges see Figure 5.

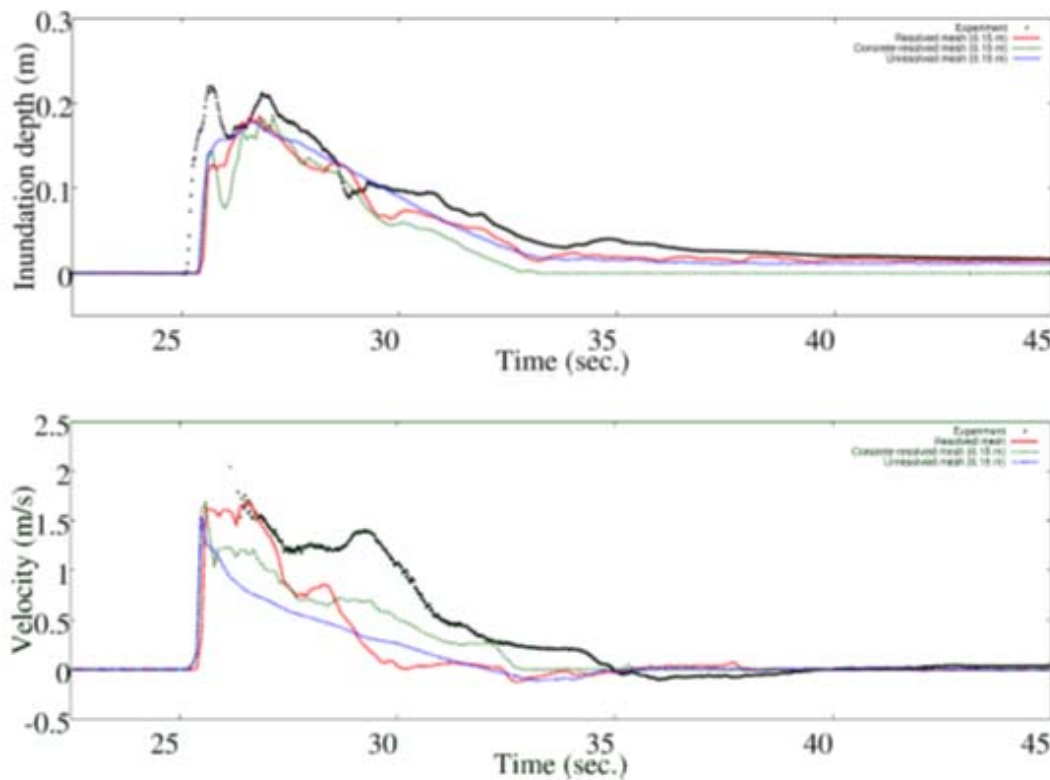


Figure 22: (Top to bottom) Flow depth and cross-shore velocity comparisons at WGB1 using FVCOM. See Table 2 and Figure 8 for the location of wave gauge.



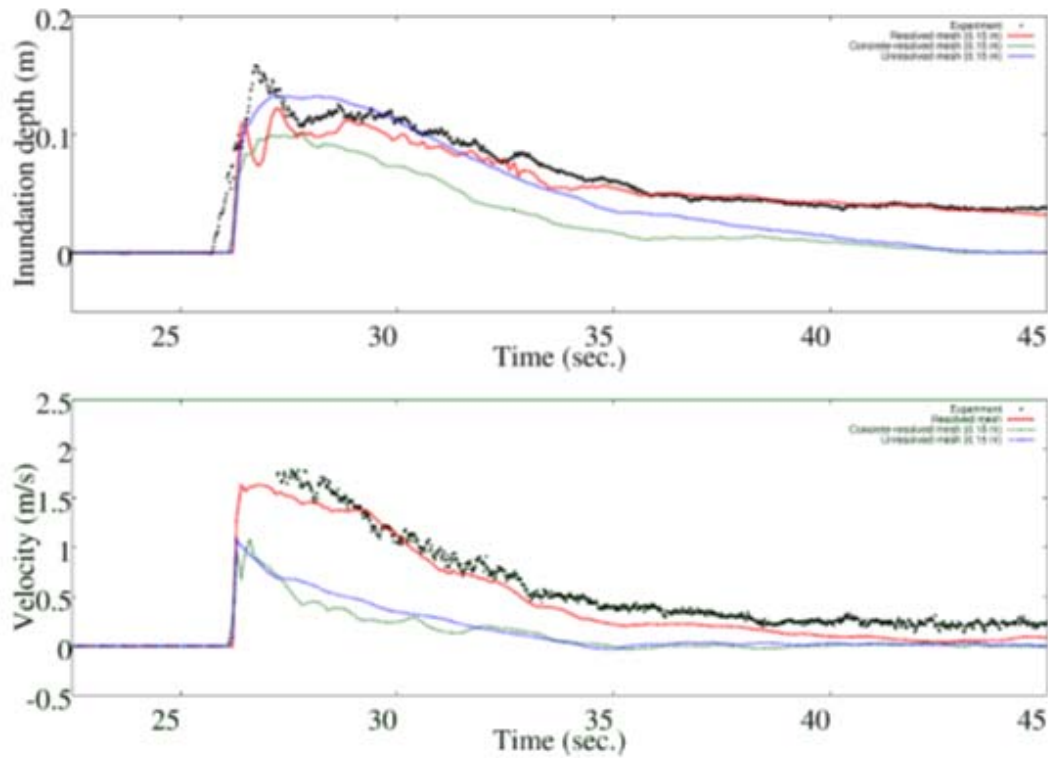


Figure 23: (Top to bottom) Flow depth and cross-shore velocity comparisons at WGB4 using FVCOM. See Table 2 and Figure 8 for the location of wave gauge.



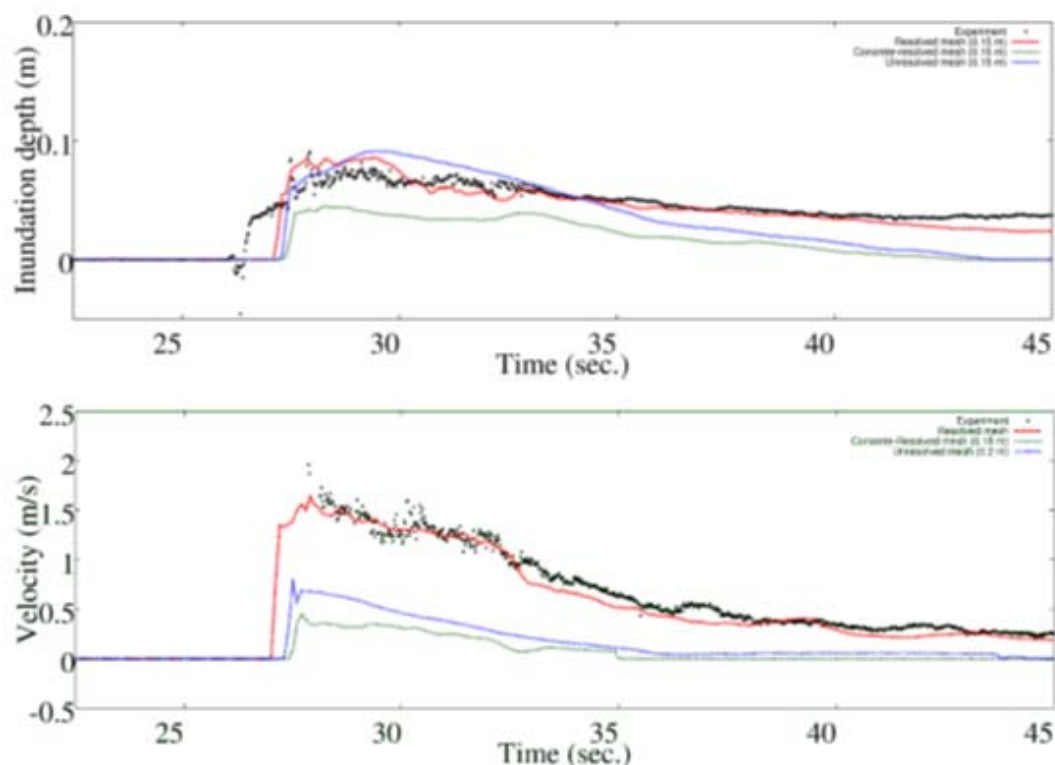


Figure 24: (Top to bottom) Flow depth and cross-shore velocity comparisons at WGB6 using FVCOM. See Table 2 and Figure 8 for the location of wave gauge.

References

- American Society of Civil Engineers (ASCE), Structural Engineering Institute (2016). Minimum Design Loads for Buildings and Other Structures, ASCE/SEI 7-16 (in preparation for publication).
- Borero, J., Ortiz, M., Titov, V., and Synolakis, C. (1997). Field survey of Mexican tsunami produces new data, unusual photos. EOS Transactions American Geophysical Union, 78, 85–88. doi:10.1029/97EO00054
- Carrier, G.F., Wu, T.T., and Yeh, H. (2003). Tsunami runup and drawdown on a plane beach. J. Fluid Mech., 475, 79–99.
- Chen, C., Beardsley, R.C., and Cowles, G. (2006). An unstructured grid, Finite-Volume Coastal Ocean Model (FVCOM) User Manual Second Edition.
- FEMA 2000. Coastal Construction Manual. FEMA 55, Federal Emergency Management Agency.
- Fritz, H.M., Borrero, J.C., Synolakis, C.E., and Yoo, J. (2006). 2004 Indian Ocean tsunami flow velocity measurements from survivor videos. Geophys. Res. Lett., 33(24), Art. No. L24605. doi:10.1029/2006GL026784



Fryer, G.J., Watts, P., and Pratson, L.F. (2004). Source of the great tsunami of 1 April, 1946: a landslide in the upper Aleutian forearc. *Marine Geology*, 203, 201–218.

Kânoğlu, U. (2004). Nonlinear evolution and runup-rundown of long waves over a sloping beach. *Journal of Fluid Mechanics*, 513, 363–372.

Kânoğlu, U., and Synolakis, C.E. (2006). Initial value problem solution of nonlinear shallow water-wave equations. *Physical Review Letters*, 97(14), 148501.

Kânoğlu, U., Sharghivand, N., Moore, C., Arcas, D., and Titov, V. (2015). Single long-period wave propagating onto a small-scale model of the town of Seaside, Oregon. Benchmark Problem #4. NTHMP - Mapping & Modeling Benchmarking Workshop: Tsunami Currents, 9-10 February 2015.

METU (2015). Existing tools, data, and literature on tsunami impact, loads on structures, failure modes and vulnerability assessment. Deliverable D1 of the RAPSODI Project. Norwegian Geotechnical Report 20120768-01-R, 108 pp. <http://www.ngi.no/en/Project-pages/RAPSODI/Reports-and-Publications/>

NAMI DANCE Manual (2010). Developed by Zaytsev, C., Yalciner, A., Pelinovsky, E., and Kurkin, A.. Tsunami Simulation/Visualization Code NAMI DANCE versions 4.9.

Okal E.A., and Hebert, H. (2007). Far-field simulation of the 1946 Aleutian tsunami. *Geophys J Int* 169:1229–1238. doi:10.1111/j.1365-246X.2007.03375.x

O'Brien, L., Christodoulides, P., Renzi, E., Stefanakis, T., and Dias, F. (2015). Will oscillating wave surge converters survive tsunamis? *Theoretical & Applied Mechanics Letters* (in print).

Park, H., Cox, D., Lynett, P., Wiebe, D., and Shin, S. (2013) Tsunami Inundation Modeling in Constructed Environments: A Physical and Numerical Comparison of Free-Surface Elevation, Velocity, and Momentum Flux. *Coastal Engineering*, 79, 9–21. doi: 10.1016/j.coastaleng.2013.04.002.

Sumer, B.M., Ansal, A., Cetin, K.O., Damgaard, J., Gunbak, A.R., Ottesen Hansen, N-E., Sawicki, A., Synolakis, C.E., Yalciner, A.C., Yuksel, Y., and Zen, K. (2007). Earthquake-induced liquefaction around marine structures. *Journal of Waterway Port, Coastal and Ocean Engineering*, 133(1), 55–82. doi: 10.1061/(ASCE)0733-950X(2007)133:1(55)

Synolakis, C.E., Bernard, E.N., Titov, V.V., Kânoğlu, U., and González, F.I. (2008). Validation and verification of tsunami numerical models. *Pure and Applied Geophysics*, 165, 2197–2228. doi:10.1007/s00024-004-0427-y

Synolakis, C.E., Bernard, E.N., Titov, V.V., Kânoğlu, U., and González, F.I. (2007). Standards, criteria, and procedures for NOAA evaluation of tsunami numerical models. Technical Report OAR PMEL-135, NTIS: PB2007-109601 The National Oceanic and Atmospheric Administration.

Synolakis, C.E. (2003). Tsunami and Seiche. In: Chen, W.F. and Scawthorn, C. (eds.). *Earthquake Engineering Handbook*. CRC Press, New York, 9–1 to 9–99.

NGI



Synolakis, C.E. (1987). The runup of solitary waves. *Journal Fluid Mechanics*, 185, 523–545. doi:10.1017/S002211208700329X

Synolakis, C.E. (1986). The runup of long waves. Ph.D. thesis, California Institute of Technology, Pasadena, California 91125, p. 228.

Titov, V., and Synolakis, C. (1995). Modeling of breaking and nonbreaking long-wave evolution and runup using VTCS-2. *Journal of Waterway Port Coastal and Ocean Engineering-ASCE*, 121, 308–316. doi:10.1061/(ASCE) 0733-950X(1995)121:6(308)

Titov, V., and Synolakis, C. (1997). Extreme inundation flows during the Hokkaido-Nansei-Oki tsunami. *Geophysical Research Letters*, 24, 1315–1318. doi:10.1029/97GL01128

Titov, V., and Synolakis, C. (1998). Numerical modeling of tidal wave runup. *Journal of Waterway Port Coastal and Ocean Engineering-ASCE*, 124, 157–171. doi:10.1061/(ASCE)0733-950X(1998)124:4(157)

Wiyono, R.U.A. (2015). Unstructured mesh tsunami simulation using FVCOM considering the fine structure of land use. PhD Thesis. Yokohama National University.

Yalçın, A.C., Zaytsev, A., Kânoğlu, U., Dogan, G.G., Velioğlu, D., Kian, R., Aytore, B., Sharghivand, N. (2015). NAMI DANCE benchmark results. NTHMP Workshop report (in preparation for publication).

Yeh, H., Robertson, I., and Preuss, J. (2005). Development of design guidelines for structures that serve as tsunami vertical evacuation sites. Technical report, Washington Division of Geology and Earth Resources.

Yeh, H. (2006). Tsunami Forces in the Runup Zone. NSF Caribbean Tsunami Workshop, World Scientific, Editors: Mercado-Irizarry, A., Liu, P., 275–287

Zelt, J.A., and Raichlen, F. (1991). Overland flow from solitary waves. *Journal Waterway Port C-ASCE*, 117(3), 247–263. doi:10.1061/(ASCE)0733-950X(1991)117:3(247)



Review and reference page

Document information					
Document title Deliverable D5 Report on computed tsunami parameter values in shallow waters and around structures (month 16 METU)			Document No. 20120768-05-R		
Type of document Report		Distribution Limited		Date 30 June 2015	
				Rev. No & date	
Client CONCERT-Japan Joint Call Secretariat					
Keywords					
Geographical information					
Country, County			Offshore area		
Municipality			Field name		
Location			Location		
Map			Field, Block No.		
UTM-coordinates					
Document control					
Quality assurance according to NS-EN ISO9001					
Rev.	Reason for revision	Self review by:	Colleague review by:	Independent review by:	Inter-disciplinary review by:
0	Original document				
Document approved for release		Date 30 June 2015		Sign. Project Manager Carl B. Harbitz	

NGI



**Middle East
Technical University**
Civil Engineering
Department



CONCERT JAPAN
Connecting and Coordinating
European Research and Technology Development with Japan
concertjapan.eu